The Astrophysical Journal, 954:186 (10pp), 2023 September 10 https://doi.org/10.3847/1538-4357/acea5d


# On the Properties of Inverse Compton Spectra Generated by Upscattering a Power-law Distribution of Target Photons

Dmitry Khangulyan[1], Felix Aharonian[2,3,4], and Andrew M. Taylor[5]
[1] Graduate School of Artificial Intelligence and Science, Rikkyo University, Nishi-Ikebukuro 3-34-1, Toshima-ku, Tokyo 171-8501, Japan
d.khangulyan@rikkyo.ac.jp
[2] Dublin Institute for Advanced Studies, School of Cosmic Physics, 31 Fitzwilliam Place, Dublin 2, Ireland
[3] Max-Planck-Institut für Kernphysik, Saupfercheckweg 1, D-69117 Heidelberg, Germany
[4] Yerevan State University, 1 Alek Manukyan Street, Yerevan 0025, Armenia
[5] DESY, D-15738 Zeuthen, Germany
*Received 2023 May 5; revised 2023 July 23; accepted 2023 July 23; published 2023 September 6*

## Abstract

Relativistic electrons are an essential component in many astrophysical sources, and their radiation may dominate the high-energy bands. Inverse Compton (IC) emission is the radiation mechanism that plays the most important role in these bands. The basic properties of IC, such as the total and differential cross sections, have long been studied; the properties of the IC emission depend strongly not only on the emitting electron distribution but also on the properties of the target photons. This complicates the phenomenological studies of sources, where target photons are supplied from a broad radiation component. We study the spectral properties of IC emission generated by a power-law distribution of electrons on a power-law distribution of target photons. We approximate the resulting spectrum by a broken-power-law distribution and show that there can be up to three physically motivated spectral breaks. If the target photon spectrum extends to sufficiently low energies, $\varepsilon_{\rm min} < m_e^2c^4/E_{\rm max}$ ($m_e$ and $c$ are electron mass and speed of light, respectively; $\varepsilon_{\rm min}$ and $E_{\rm max}$ are the minimum/maximum energies of target photons and electrons, respectively), then the high-energy part of the IC component has a spectral slope typical for the Thomson regime with an abrupt cutoff close to $E_{\rm max}$. The spectra typical for the Klein–Nishina regime are formed above $m_e^2c^4/\varepsilon_{\rm min}$. If the spectrum of target photons features a cooling break, i.e., a change of the photon index by 0.5 at $\varepsilon_{\rm br}$, then the transition to the Klein–Nishina regime proceeds through an intermediate change of the photon index by 0.5 at $m_e^2c^4/\varepsilon_{\rm br}$.

*Unified Astronomy Thesaurus concepts:* Gamma-ray sources (633); Gamma-ray bursts (629); Gamma-ray transient sources (1853); Gamma-rays (637)

## 1. Introduction

Inverse Compton (IC) scattering together with synchrotron emission are essential leptonic radiation mechanisms. Synchrotron–IC models often provide very good fits to broadband observations for astrophysical sources containing ultrarelativistic electrons. Calculating synchrotron-IC spectral energy distributions (SEDs) is a standard task in high-energy astrophysics thanks to detailed theoretical descriptions (for a review see Blumenthal & Gould 1970) and convenient software packages (e.g., `naima` by Zabalza 2015). The standard treatment of magnetobremsstrahlung emission is based on a well-known formula from classical electrodynamics that describes the electromagnetic field of a charge gyrorating in a homogeneous magnetic field, leading to the generation of synchrotron radiation. If the magnetic field has chaotically distributed directions, the emission spectrum remains essentially unchanged (Crusius & Schlickeiser 1986; Aharonian et al. 2010). This is, however, not a general result. If the magnetic field additionally features significant fluctuations in its strength, then the standard synchrotron emission spectrum can be considerably modified (Kelner et al. 2013; Derishev & Aharonian 2019). Furthermore, if the emission is generated within small-scale turbulence, in the so-called jitter regime, the produced spectra deviates strongly from that expected in the conventional synchrotron regime (see in Kelner et al. 2013, and references therein). Finally, the synchrotron approximation is not applicable when the emitting particle moves at a small pitch angle to the magnetic field, such that the curvature of the trajectory of the particle is determined by the curvature of the magnetic field lines (Cheng & Zhang 1996; Kelner et al. 2015); or when the particle interacts with the magnetic field in the quantum regime (e.g., Schwinger 1954). Despite these physically motivated exceptions, standard synchrotron emission remains an almost universal approximation for the magnetobremsstrahlung radiation channel.

In the case of IC scattering, the situation is quite different, and the distribution of the target photons plays a critical role almost in all astrophysical scenarios. Therefore, to obtain the SED of IC radiation one needs to convolve the differential cross section with the energy and angular distribution of the target photons. The anisotropic differential cross section for IC scattering is available in the literature (Aharonian & Atoyan 1981). It can be readily used for obtaining the IC emission generated by an electron on a monoenergetic beam of photons. If photons have energy and/or angular distribution one can numerically integrate over the photon spectrum or use some analytical derivations available in the literature. These include, for example, the IC cross section averaged over the scattering angle (Jones 1968), and convolution with a Planckian energy distribution of the target photons (Khangulyan et al. 2014).

In what follows, we qualitatively discuss the properties of IC emission generated on a power-law distribution of target photons. While numerically computing the corresponding IC spectrum is still a simple task, we focus on finding the key factors that determine the spectral properties. Our findings simplify the phenomenological analysis of broadband spectra from gamma-ray sources that feature bright X-ray emission. For example, the results obtained can be used for studying gamma-ray bursts (GRBs) and flares associated to relativistic outflows from active galactic nuclei (AGN). The manuscript is organized as follows: in Section 2 we summarize the properties of IC scattering and introduce several simple approximations that allow the calculation of the IC loss rates and the mean upscattered photon energy; in Section 3, using the $\delta$-function approximation for the single-electron emissivity, we reveal the key factors that determine the spectral properties of IC component generated on a broad power-law distribution of target photons; and we discuss our findings in Section 4.

## 2. Compton Scattering

The cross section, $\sigma_{\rm ic}$, describing the scattering of photons by an electron can be obtained with the standard means of quantum electrodynamics. If scattering proceeds in a mono-directional beam of target photons that have energy of $\varepsilon$, then for a single electron the scattering rate, $\dot{N}_{\rm ani}$, is given by the usual expression

$$\dot{N}_{\rm ani} = c(1 - v_e \cos\theta)\sigma_{\rm ic} n_{\rm ph}. \quad (1)$$

Here, $c$ is speed of light; $\theta$ is the angle between the beam direction and the electron velocity; and $v_e$ is electron speed in speed of light units ($v_e \approx 1$ for ultrarelativistic electrons); and $n_{\rm ph}$ is the number of target photons per unit of volume in the laboratory frame. The cross section is given by the following expression (see, e.g., Berestetskii et al. 1982):

$$\sigma_{\rm ic} = \frac{3\sigma_{\rm T}}{4b_\theta}\left[\left(1 - \frac{4}{b_\theta} - \frac{8}{b_\theta^2}\right)\log(1 + b_\theta) + \frac{1}{2} + \frac{8}{b_\theta} - \frac{1}{2(1 + b_\theta)^2}\right], \quad (2)$$

where $b_\theta = 2E\varepsilon(1 - v_e\cos\theta)/(m_e^2c^4)$ is a parameter that determines the scattering regime; $\sigma_{\rm T} = 8\pi r_e^2/3$ is the Thomson cross section (here $r_e = e^2/(m_e c^2)$ is the electron classical radius and $m_e$ is electron mass). For the sake of simplicity, in what follows we set $v_e$=1. For $b_\theta \ll 1$ and $b_\theta \gg 1$ the scattering proceeds in the Thomson and Klein–Nishina regimes, respectively. Since $b_\theta$ is a Lorentz invariant (indeed, $b_\theta \propto (pk)$, where $p$ and $k$ are four-momenta of interacting electron and photon, respectively), the scattering regime does not depend on the choice of the reference frame.

In any realistic configuration, the target photons have some energy and/or angular distribution: $dn_{\rm ph} = n_{\rm ph}(\varepsilon, \boldsymbol{n})d\varepsilon d\Omega_{\boldsymbol{n}}$, where $d\Omega_{\boldsymbol{n}}$ is solid angle element in the direction of the photons' momentum, $\boldsymbol{n}$. To obtain the scattering rate, one needs to integrate over the photon distribution:

$$\dot{N} = c\int(1 - \cos\theta)\sigma_{\rm ic} n_{\rm ph}(\varepsilon, \boldsymbol{n})d\varepsilon d\Omega_{\boldsymbol{n}}. \quad (3)$$

Here, $\theta$ is the angle between the electron's initial velocity vector and $\boldsymbol{n}$. In the relativistic case it is safe to assume that the upscattered photon propagates in the direction of the electron's initial velocity vector; thus the angular distribution of upscattered photons is determined both by the electron and target photon distributions.

If the target photons are isotropically distributed in the laboratory frame $n_{\rm ph}(\varepsilon, \boldsymbol{n}) = n_{\rm ph}(\varepsilon)/(4\pi)$, then the integration over the angular variables can be performed analytically:

$$\dot{N}_{\rm iso} = c\int d\varepsilon n_{\rm ph}(\varepsilon)\left[\frac{1}{4\pi}\int(1 - \cos\theta)\sigma_{\rm ic}(b_\theta)d\Omega_{\boldsymbol{n}}\right], = c\int d\varepsilon n_{\rm ph}(\varepsilon)\bar{\sigma}_{\rm ic}(b), \quad (4)$$

where $b = 4E\varepsilon/(m_e^2c^4)$ is a dimensionless parameter. We note that the energies $E$ and $\varepsilon$ are written in the specific reference frame in which the photon field is isotropic.

The cross section averaged over the scattering angle can be computed analytically yielding a relatively simple expression that, however, contains a dilogarithm function:

$$\bar{\sigma}_{\rm ic} = \frac{3\sigma_{\rm T}}{2b^2} \times \left(\frac{b^2 + 9b + 8}{b}\log(b + 1) + \frac{2 - b^2}{2(b + 1)} - 9 + 4{\rm Li}_2(-b)\right). \quad (5)$$

Here $\rm Li_2$ is dilogarithm function defined as ${\rm Li}_2(x) = \int_x^0 dt\frac{\log(1-t)}{t}$. We introduce an auxiliary function $F_{\rm n,iso}$ by factoring out the dependence on $b$ as $\bar{\sigma}_{\rm ic} = \sigma_{\rm T}F_{\rm n,iso}(b)$. The asymptotic behavior of this function is

$$F_{\rm n,iso} = \begin{cases} 1, & b \ll 1 \\ \dfrac{3}{2b}\log(b), & b \gg 1. \end{cases} \quad (6)$$

Similar to Khangulyan et al. (2014), we suggest the following approximate representation for the function $F_{\rm n,iso}$:

$$G^{(0)}_{\rm n,iso} = \frac{3}{2b}\log\left(1 + \frac{2}{3}b\right). \quad (7)$$

This simple function provides a rough approximation for $F_{\rm n,iso}$, with a relative error at the level of 20%. If a higher precision is needed, and using the original analytic expression given by Equation (5) is not convenient (e.g., because of the presence of dilogarithm function), then the approximation can be improved with the standard correction function from Khangulyan et al. (2014):

$$g_i(x) = \left[1 + \frac{a_i x^{\alpha_i}}{1 + b_i x^{\beta_i}}\right]^{-1}. \quad (8)$$

For example, for the following parameters $\alpha_i = 0.89$, $a_i = 0.24$, $\beta_i = 1.36$, and $b_i = 0.4$, function

$$G_{\rm n,iso} = G^{(0)}_{\rm n,iso} \times g_i \quad (9)$$

approximates the analytical expression for the scattering rate, Equation (5), with an accuracy of better than 0.7%.

While the total cross section has a relatively simple mathematical form, obtaining the differential cross section is a more challenging task. The differential cross section, $d\sigma_{\rm ic}/d\omega$, defines the rate of upscattering of target photons with energy $\varepsilon$ in to the energy interval of $(\omega, \omega + d\omega)$. For astrophysical applications, the general expressions for the differential cross section can be significantly simplified using the fact that the energy of the target photons is typically small,

$\varepsilon \ll m_e c^2$, and the electrons are relativistic, $E \gg m_e c^2$. Under these assumptions, for a monodirectional beam of target photons, the scattering rate by an electron moving with a velocity that makes an angle $\theta$ with the photon's direction has the following simple form (Aharonian & Atoyan 1981):

$$\dot{n}_{\rm ani}(\omega) = c(1-\cos\theta) d\sigma_{\rm ic}\omega n_{\rm ph}, \tag{10}$$

where $\dot{n}_{\rm ani}(\omega) = d\dot{N}_{\rm ani}/d\omega$ and

$$d\sigma_{\rm ic}\omega = \frac{3\sigma_{\rm T}}{2b_\theta E} \times \left[1 + \frac{z^2}{2(1-z)} - \frac{2z}{b_\theta(1-z)} + \frac{2z^2}{b_\theta^2(1-z)^2}\right]. \tag{11}$$

Here $z = \omega/E$ is the ratio of the upscattered photon energy to the initial electron energy. If the target photon field is isotropic, the above expression should be averaged over the interaction angle:

$$\dot{n}_{\rm iso}(\omega) = c\int (1-\cos\theta) d\sigma_{\rm ic}\omega \frac{d\Omega_{\boldsymbol{n}}}{4\pi} n_{\rm ph} = c d\bar{\sigma}_{\rm ic}\omega n_{\rm ph}. \tag{12}$$

Here $\dot{n}_{\rm iso}(\omega) = d\dot{N}_{\rm iso}/d\omega$ and $d\bar{\sigma}_{\rm ic}/d\omega$ is the angle-averaged cross section (Jones 1968):

$$d\bar{\sigma}_{\rm ic}\omega = \frac{3\sigma_{\rm T}}{bE} \times \left[1 + \frac{z^2}{2(1-z)} + \frac{z}{b(1-z)} - \frac{2z^2}{b^2(1-z)^2} - \frac{z^3}{2b(1-z)^2} - \frac{2z}{b(1-z)} \log\frac{b(1-z)}{z}\right]. \tag{13}$$

The differential cross section is used to compute the gamma-ray spectrum produced by an electron distribution, $dN_e = n_e dE$, in the anisotropic and isotropic regimes:

$$\dot{n}^{\rm tot}_{\rm ani}(\omega) = c\int (1-\cos\theta) d\sigma_{\rm ic}\omega n_e(E) n_{\rm ph}(\varepsilon) dE d\varepsilon$$
$$\dot{n}^{\rm tot}_{\rm iso}(\omega) = c\int d\bar{\sigma}_{\rm ic}\omega n_e(E) n_{\rm ph}(\varepsilon) dE d\varepsilon. \tag{14}$$

Another important aspect is that the differential cross section allows one to obtain the IC energy losses of an electron:

$$\dot{E}_{\rm ani} = -c\int (1-\cos\theta)(\omega-\varepsilon) d\sigma_{\rm ic}\omega n_{\rm ph}(\varepsilon) d\omega d\varepsilon,$$
$$\dot{E}_{\rm iso} = -c\int (\omega-\varepsilon) d\bar{\sigma}_{\rm ic}\omega n_{\rm ph}(\varepsilon) d\omega d\varepsilon, \tag{15}$$

where the integration over $\omega$ is performed in the range allowed by the kinematic constraints:

$$\omega_{\rm max/min} = \omega_{\rm cms}\Gamma_{\rm cms}(1 \pm v_{\rm cms}). \tag{16}$$

Here, quantities with subscript "cms" are evaluated in the center-of-mass (CMS) reference frame:

$$\omega_{\rm cms} = \frac{1}{2}\frac{m_e c^2 b_\theta}{\sqrt{1+b_\theta}},$$
$$\Gamma_{\rm cms} = \frac{E+\omega}{m_e c^2\sqrt{1+b_\theta}},$$
$$v_{\rm cms} = \sqrt{1-\Gamma_{\rm cms}^{-2}}. \tag{17}$$

For relativistic electrons in Equation (15) it is safe to use the following approximations:

$$\omega_{\rm min} \approx 0,$$
$$\omega_{\rm max} \approx E\frac{b_\theta}{1+b_\theta},$$
$$\omega - \varepsilon \approx \omega. \tag{18}$$

Note that if an electron interacts with an isotropic photon field, then in Equation (18) one should replace $b_\theta$ with $b$ as the upscattered photon energy is maximal for $\theta = \pi$.

IC energy losses on a monoenergetic beam of photons, $n_{\rm ph}(\varepsilon) = n_0\delta(\varepsilon-\varepsilon_0)$, can be obtained from Equation (15) by an elementary integration:

$$\dot{E}_{\rm ani} = -\frac{3\sigma_{\rm T} c n_0 E(1-\cos\theta)}{2b_\theta^2} \times \left(\left(\frac{b_\theta}{2} - 2 - \frac{6}{b_\theta}\right)\log(1+b_\theta) + \frac{3b_\theta^2+11b_\theta+6}{12(b_\theta+1)^3} + \frac{11}{2} - \frac{5}{12}b_\theta\right), \tag{19}$$

where $b_\theta = 2E\varepsilon_0(1-\cos\theta)/(m_e^2c^4)$. According to Jones (1968), IC energy losses on a monoenergetic isotropic distribution of photons is

$$\dot{E}_{\rm iso} = -\frac{3\sigma_{\rm T} c n_0 E}{b^2} \times \left\{\left(\frac{1}{2}b + 6 + \frac{6}{b}\right)\log(1+b) - \frac{\left[\frac{11}{12}b^3 + 6b^2 + 9b + 4\right]}{(1+b)^2} - 2 + 2{\rm Li}_2(-b)\right\},$$
$$= -\sigma_{\rm T} c n_0 E F_{\rm iso}(b), \tag{20}$$

where $b = 4\varepsilon_0 E/(m_e^2c^4)$. The asymptotic behavior of $F_{\rm iso}$ is

$$F_{\rm iso} = \begin{cases} \frac{b}{3}, & b \ll 1 \\ \frac{3}{2b}\log(b), & b \gg 1. \end{cases} \tag{21}$$

Similarly to Khangulyan et al. (2014), we suggest the following approximate representation for the function $F_{\rm iso}$

$$G^{(0)}_{\rm iso} = \frac{3c_{\rm iso}\log(1+0.111b/c_{\rm iso})}{1+2c_{\rm iso}\,b}. \tag{22}$$

Here $c_{\rm iso}$ is a numerical factor, which does not change the asymptotic behavior. For example, for $c_{\rm iso} = 0.785$, function $G^{(0)}_{\rm iso}$ follows function $F_{\rm iso}$ within 2% margin. This very simple approximation likely provides an accuracy sufficient for any astrophysical application. If a higher precision is needed, one can use the original analytic expression given by Equation (20) or improve the approximation with the correction function Equation (8). For example, for the following parameters $c_{\rm iso} = 0.87$, $a_i = -0.275$, $\alpha_i = 1.02$, $b_i = 4.24$, $\beta_i = 1.1$, function

$$G_{\rm iso} = G^{(0)}_{\rm iso} \times g_i \tag{23}$$

approximates the analytic expression for IC losses, Equation (20), with accuracy better than 0.3%. Comparison

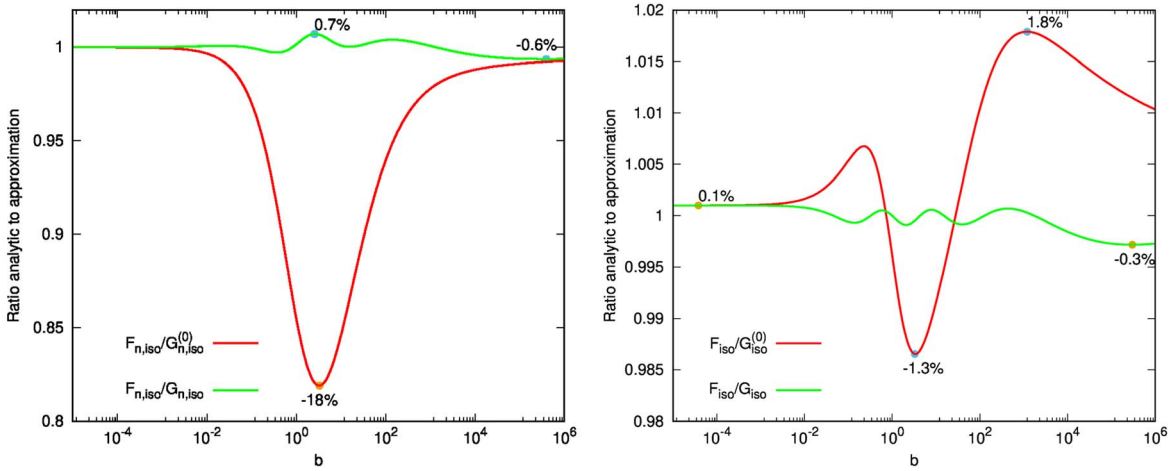


**Figure 1.** Top panel: the ratio of the function $F_{\rm n,iso}$ to $G^{(0)}_{\rm n,iso}$ and $F_{\rm n,iso}$ to $G^{(0)}_{\rm n,iso} \times g_i$(for $a_i = 0.24$, $\alpha_i = 0.89$, $b_i = 0.4$, and $\beta_i = 1.36$). Bottom panel: The ratio of the function $F_{\rm iso}$ to $G^{(0)}_{\rm iso}$ (for $c_{\rm iso} = 0.785$) and $F_{\rm iso}$ to $G^{(0)}_{\rm iso} \times g_i$(for $c_{\rm iso} = 0.87$, $a_i = -0.275$, $\alpha_i = 1.02$, $b_i = 4.24$, and $\beta_i = 1.1$).

of approximations with the analytic expression is shown in Figure 1.

The mean photon energy can be obtained from the energy loss and scattering rates:

$$\bar{\omega}_{\rm iso}(E,\,\varepsilon) = \frac{\dot{E}_{\rm iso}}{\dot{N}_{\rm iso}} = E\frac{F_{\rm iso}(b)}{F_{\rm n,iso}(b)}. \tag{24}$$

In the Thomson and Klein–Nishina regimes, this yields the well-known asymptotic expressions

$$\frac{\bar{\omega}_{\rm iso}}{E} = \begin{cases} b/3 \text{ if } b \ll 1, \\ 1 \text{ if } b \gg 1. \end{cases} \tag{25}$$

To express the mean photon energy in the transition regions, Equation (24) can be approximated as

$$\frac{\bar{\omega}_{\rm iso}(E,\,\varepsilon)}{E} \approx \frac{G^{(0)}_{\rm iso}(b)}{G^{(0)}_{\rm n,iso}(b)}, \tag{26}$$

which can be further reduced to the simple expression,

$$\frac{\bar{\omega}_{\rm iso}(E,\,\varepsilon)}{E} \approx \frac{6b/5}{1+6b/5}\frac{\log(1+5b/27)}{\log(1+2b/3)}. \tag{27}$$

This provides a better than 2% approximation for the upscattered photon energy in the entire energy range.

A similar expression is available for the anisotropic scattering regime. In this case, the asymptotic behavior is

$$\frac{\bar{\omega}_{\rm ani}}{E} = \begin{cases} b_\theta/2 & \text{if} \quad b_\theta \ll 1, \\ 1 & \text{if} \quad b_\theta \gg 1. \end{cases} \tag{28}$$

If the scattering proceeds in the anisotropic regime, the following expression provides a better than 2% approximation for the upscattered photon energy in the entire energy range

$$\frac{\bar{\omega}_{\rm ani}(E,\,\varepsilon)}{E} \approx \frac{2b_\theta}{1+2b_\theta}\frac{\log(1+b_\theta/2)}{\log(1+2b_\theta)}. \tag{29}$$

### 3. $\delta$-Function Approximation

Both in the classical Thomson and quantum Klein–Nishina regimes, a monoenergetic distribution of electrons generates a broad IC component. If the electrons themselves feature a spread in their energy distribution, then the IC component is further broadened. Once the relative width of the electron distribution exceeds the relative width of single-electron IC spectrum, the width of the single-electron IC spectrum has little influence on the total IC component, and can thus be neglected. This can be appreciated by considering IC scattering under the $\delta$-function approximation. In this $\delta$-approximation treatment, the electron energy loss rate, $\dot{E}$, and mean frequency of IC photons generated by this electron, $\bar{\omega}$, determine the emission spectrum generated by the electron (see, e.g., Felten & Morrison 1966; Kirk et al. 2005):

$$\dot{n}_{\gamma,0} = \left|\frac{\dot{E}}{\omega}\right| \delta(\omega - \bar{\omega}), \tag{30}$$

where $\dot{n}_{\gamma,0}$ is the number of photons upscattered per unit time and frequency:

$$\dot{n}_{\gamma,0} = d\dot{N}_{\gamma,0}\omega. \tag{31}$$

Equation (30) reproduces correctly the scattering rate and the radiation energy losses of the electrons emitted. The spectrum produced by an ensemble of electrons is obtained by convolution:

$$\dot{n}_\gamma = \int dE \dot{n}_{\gamma,0} n_e. \tag{32}$$

Here $n_e$ is electron energy distribution:

$$n_e = dN_e E. \tag{33}$$

Although Equations (30) and (32) can be considered an oversimplification, they still allow one to recover some basic properties of IC scattering, especially for the broadband part of the spectra far from either of the cutoff regions. For example, in the Thomson regime (see Equations (21) and (25)), the energy losses and the mean photon energy depend quadratically on energy: $\dot{E} \propto E^2$ and $\bar{\omega} \propto E^2$, respectively. If the electron distribution is a power law, $n_e \propto E^{-\alpha}$, then Equation (32) yields the standard slope of the Thomson (or synchrotron) spectra (see, e.g., Longair 2011):

$$\dot{n}_\gamma \propto \omega^{-(\alpha+1)/2}. \tag{34}$$

In the Klein–Nishina regime, the energy loss rate is constant, $\dot{E} \propto$ const (ignoring the logarithm dependence, see Equation (21)), and the mean photon energy is $\bar{\omega} \propto E$, thus for the power-law distribution of electrons one obtains (see,

e.g., in Blumenthal & Gould 1970)

$$\dot{n}_\gamma \propto \omega^{-(\alpha+1)}. \tag{35}$$

If the distribution of the target photons is sufficiently broad, then the width target spectrum needs accounting for. This can also be addressed under the $\delta$-function approximation:

$$\dot{n}_{\gamma,0} = \int \frac{1}{\omega} |d\dot{E}\varepsilon| \delta(\omega - \bar{\omega}(E, \varepsilon)) d\varepsilon, \tag{36}$$

where $d\dot{E}$ is the electron energy loss rate caused by the interaction with target photons that have their energy exclusively in the range from $\varepsilon$ to $\varepsilon + d\varepsilon$.

If the distribution of the target photons is sufficiently broad, then at least a fraction of the target photons is upscattered in the Thomson regime. Since the scattering cross section in the Klein–Nishina regime is smaller than the Thomson cross section, the part of the spectrum formed in the Thomson regime should reflect the key spectral properties. These features can be studied by setting $\bar{\omega} \propto \varepsilon E^2$ and $d\dot{E}/d\varepsilon \propto \varepsilon n_{\rm ph}(\varepsilon) E^2$, where $n_{\rm ph}$ is the energy distribution of the target photons. Thus, one obtains

$$\dot{n}_\gamma^{\rm T} \propto \int dE \int d\varepsilon \frac{1}{\omega} E^2 \varepsilon n_e(E) n_{\rm ph}(\varepsilon) \delta\left(\omega - \frac{\varepsilon E^2}{m_e^2 c^4}\right). \tag{37}$$

The integration over the $\delta$-function helps to clearly reveal the production of the broadband spectrum in the Thomson limit. Before writing the resulting equation, we note that given the presence of the $\delta$-function term, one does not need to account for the kinematic constraints on the energies of the interacting particles. However, to ensure that the scattering proceeds in the Thomson regime, we introduce a Heaviside function that determines the maximum frequency of the scattered photons: $\Theta(1 - \varepsilon E/(m_e^2 c^4))$ (note that in this section we omit some numerical factors; this, however, does not influence the conclusions). Thus, one obtains

$$\begin{aligned} \dot{n}_\gamma^{\rm T} &\propto \int dE \frac{1}{E^2} n_e(E) n_{\rm ph}\left(\frac{\omega m_e^2 c^4}{E^2}\right) \Theta(E - \omega) \\ &= \int_\omega^\infty dE \frac{1}{E^2} n_e(E) n_{\rm ph}\left(\frac{\omega m_e^2 c^4}{E^2}\right), \end{aligned} \tag{38}$$

where the lower energy limit in the integral is due to the Heaviside function, i.e., it is imposed by the Klein–Nishina cutoff, which, according to the assumptions introduced, is equivalent to an obvious requirement, $E > \omega$.

Let us assume that one deals with a power-law distributions of electrons and target photons:

$$n_e \propto E^{-\alpha} \Theta(E - E_{\rm min}) \Theta(E_{\rm max} - E) \tag{39}$$

and

$$n_{\rm ph} \propto \varepsilon^{-\beta} \Theta(\varepsilon - \varepsilon_{\rm min}) \Theta(\varepsilon_{\rm max} - \varepsilon). \tag{40}$$

Provided that $E_{\rm max} > m_e c^2 \sqrt{\omega/\varepsilon_{\rm max}}$ and $E_{\rm min} < m_e c^2 \sqrt{\omega/\varepsilon_{\rm min}}$, the integral in Equation (38) is a simple power-law function:

$$\dot{n}_\gamma^{\rm T} \propto \omega^{-\beta} \int_{\tilde{E}_{\rm min}}^{\tilde{E}_{\rm max}} dE E^{2\beta-\alpha-2}, \tag{41}$$

where the integral limits are determined by the following conditions

$$\tilde{E}_{\rm min} = \max\left(\omega, E_{\rm min}, m_e c^2 \sqrt{\frac{\omega}{\varepsilon_{\rm max}}}\right) \tag{42}$$

and

$$\tilde{E}_{\rm max} = \min\left(E_{\rm max}, m_e c^2 \sqrt{\frac{\omega}{\varepsilon_{\rm min}}}\right). \tag{43}$$

Provided $2\beta - \alpha \neq 1$ the final expression is

$$\dot{n}_\gamma^{\rm T} \propto \omega^{-\beta} \frac{1}{2\beta - \alpha - 1} (\tilde{E}_{\rm max}^{2\beta-\alpha-1} - \tilde{E}_{\rm min}^{2\beta-\alpha-1}), \tag{44}$$

where the leading term is determined by the sign of the exponent, $2\beta - \alpha - 1$.

If the sign of this exponent is positive, i.e., $\alpha < 2\beta - 1$, then the resulting spectrum is approximately

$$\dot{n}_\gamma^{\rm T} \propto \begin{cases} \omega^{-(\alpha+1)/2} & \text{if } \omega < \dfrac{\varepsilon_{\rm min} E_{\rm max}^2}{m_e^2 c^4}, \\ \omega^{-\beta} & \text{if } \omega > \dfrac{\varepsilon_{\rm min} E_{\rm max}^2}{m_e^2 c^4}. \end{cases} \tag{45}$$

Thus, it can be seen that the spectrum keeps the same slope as that predicted by the standard Thomson estimate. If the IC spectrum extends into the energy range where the lower energy part of the spectrum does not make any contribution, $\omega > \varepsilon_{\rm min} E_{\rm max}^2/(m_e^2 c^4)$, the IC spectrum is determined by the slope of the target photons, $\dot{n}_\gamma^{\rm T} \propto \omega^{-\beta}$. The relation between the parameters is graphically shown in Figure 2.

A similar effect defines the slope of the low-energy part of the IC spectrum if $\alpha > 2\beta - 1$. In this case, the high-energy part of the target photon spectrum provides the most important contribution, and the slope of IC emission is inherited from the target photon spectrum if $\omega < \varepsilon_{\rm max} E_{\rm min}^2/(m_e^2 c^4)$ and $\omega < E_{\rm min}$. The dependence of $\tilde{E}_{\rm min}$ on $\omega$ is sketched out in Figure 3. If $E_{\rm min} > m_e^2 c^4/\varepsilon_{\rm max}$ the IC spectrum directly translates from $\omega^{-\beta}$ to $\omega^{-\alpha+\beta-1}$ at $\omega = E_{\rm min}$. If $E_{\rm min} < m_e^2 c^4/\varepsilon_{\rm max}$ the transition between these two regimes proceeds through $\omega^{-(\alpha+1)/2}$, which is realized for $\varepsilon_{\rm max} E_{\rm min}^2/(m_e^2 c^4) < \omega < m_e^2 c^4/\varepsilon_{\rm max}$. These spectral properties are summarized by the following expressions (see also Figure 3):

$$\dot{n}_\gamma^{\rm T} \propto \begin{cases} \omega^{-\beta} & \text{if } \omega < \dfrac{\varepsilon_{\rm max} E_{\rm min}^2}{m_e^2 c^4} \text{ and } \omega < E_{\rm min}, \\ \omega^{-(\alpha+1)/2} & \text{if } \omega > \dfrac{\varepsilon_{\rm max} E_{\rm min}^2}{m_e^2 c^4} \text{ and } \omega < \dfrac{m_e^2 c^4}{\varepsilon_{\rm max}}, \\ \omega^{-(\alpha+1)+\beta} & \text{if } \omega > E_{\rm min} \text{ and } \omega > \dfrac{m_e^2 c^4}{\varepsilon_{\rm max}}. \end{cases} \tag{46}$$

The resultant IC spectra obtained by numerical integration of the differential cross section over power-law distributions of target photons and electrons are shown in Figures 4 and 5. The simple analytic dependencies shown in the figures are given by Equations (45) and (46). Also, it can be seen from Figure 5 that Equation (35) describes the spectral slope in the part of the spectrum generated in the Klein–Nishina regime.

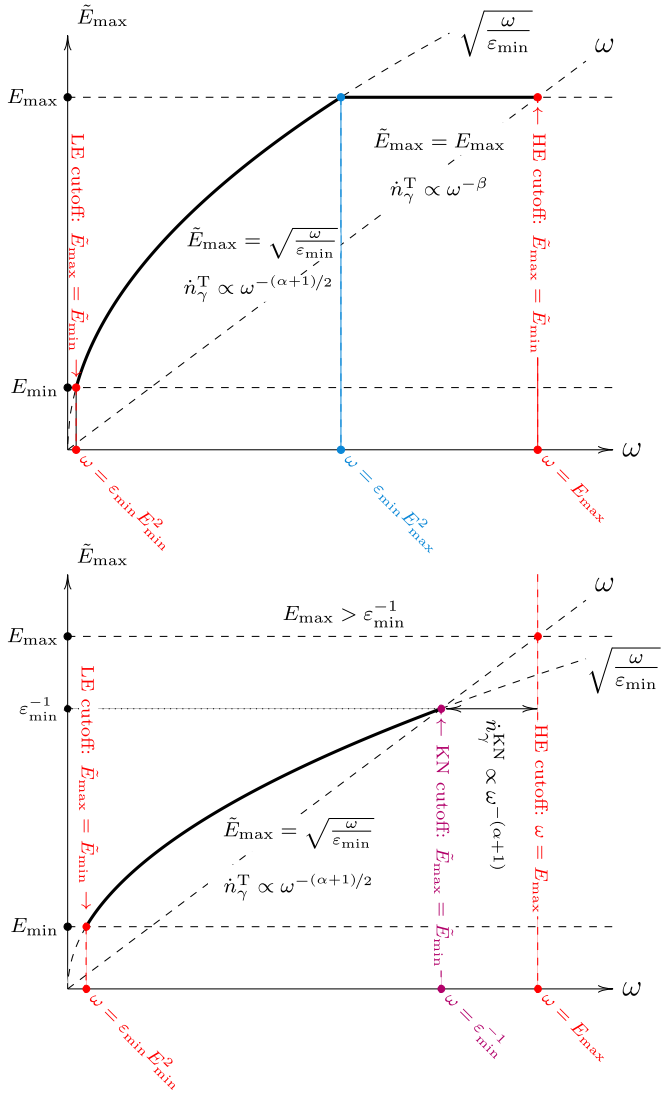


**Figure 2.** Dependence of $\tilde{E}_{\rm max}$ from Equation (43) on the upscattered photon energy together with the conditions that determine the cutoff energy. Note that in the figure labels we omit $m_{ec}^2$ factors.

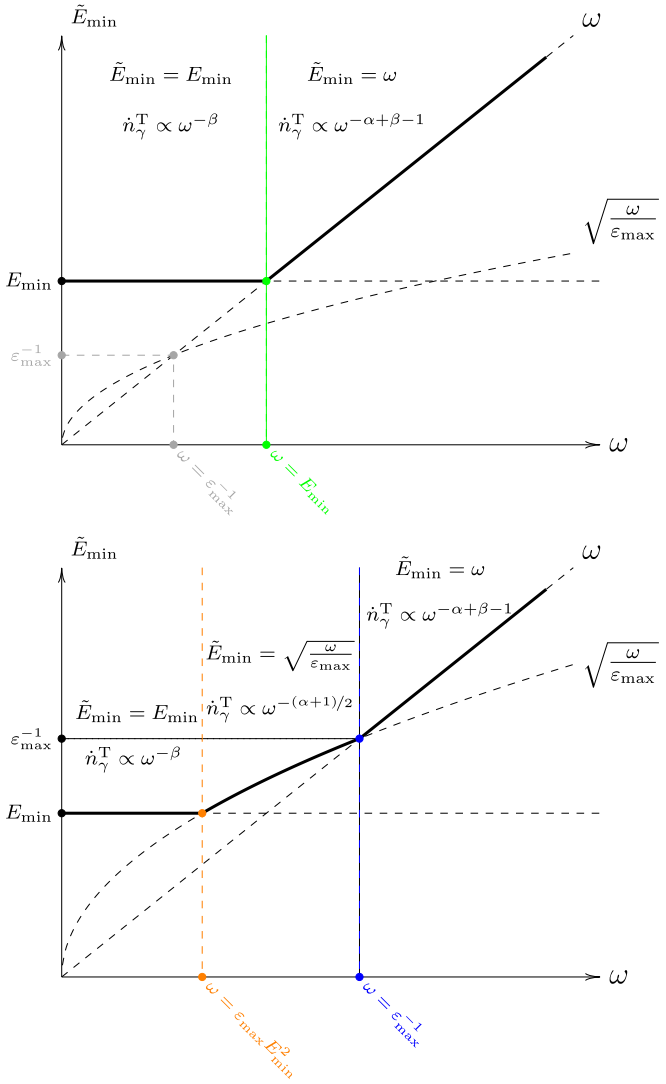


**Figure 3.** Dependence of $\tilde{E}_{\rm min}$ from Equation (42) on the upscattered photon energy. Note that in the figure labels we omit $m_{ec}^2$ factors.

Another important question is in which energy interval the revealed power-law dependencies are relevant. The approach used is relevant if the integration interval is sufficiently broad. Thus, the condition of the applicability of the obtained results is

$$\tilde{E}_{\rm min} \ll \tilde{E}_{\rm max}. \tag{47}$$

Once the integral limits approach each other, the power-law behavior becomes distorted, and the integral in Equation (41) starts to vanish, i.e., the condition $\tilde{E}_{\rm min} \sim \tilde{E}_{\rm max}$ defines the position of the spectral cutoffs. The low-energy cutoff is then simply given by the condition

$$\omega_{\rm min} \approx \frac{\varepsilon_{\rm min} E_{\rm min}^2}{m_e^2 c^4}. \tag{48}$$

For the high-energy cutoff, the determination of the conditions is a little more involved. Unless the parameters are tuned, it is natural to expect that in the high $\omega$ regime the low-energy limit of the integral, Equation (42), is simply $\omega$. The upper bound can be either $E_{\rm max}$ or $m_e c^2 \sqrt{\frac{\omega}{\varepsilon_{\rm min}}}$ (see in Figure 2 for a sketch). In the former case, the disappearance of the integral is caused by $\omega \to E_{\rm max}$ and the spectrum should completely disappear at $E_{\rm max}$. This is shown by the IC spectrum computed for $E_{\rm max} = 100$ GeV in the bottom panel of Figure 4.

In the case when $E_{\rm max} > m_e^2 c^4/\varepsilon_{\rm min}$, one should expect a transition to the Klein–Nishina regime when $\omega \to m_e c^2 \sqrt{\frac{\omega}{\varepsilon_{\rm min}}}$. This means that at the gamma-ray energy

$$\omega_{\rm kn} \sim \frac{m_e^2 c^4}{\varepsilon_{\rm min}}, \tag{49}$$

the IC spectrum should obtain a typical slope for the Klein–Nishina regime: $\dot{n}_\gamma \propto \omega^{-(\alpha+1)}$ (see in Figure 2). This transformation is illustrated by curves computed for $\varepsilon_{\rm min} = 10$ eV in Figures 4 and 5.

However, we note that the IC spectra can appear significantly harder than that expected to be produced via interactions in the Klein–Nishina regime, if the distribution of target photons extends to sufficiently low energies (i.e., the condition given by Equation (49) is not fulfilled—see the spectra computed for $\varepsilon_{\rm min} = 10^{-3}$ eV in the top panels of Figures 4 and 5).

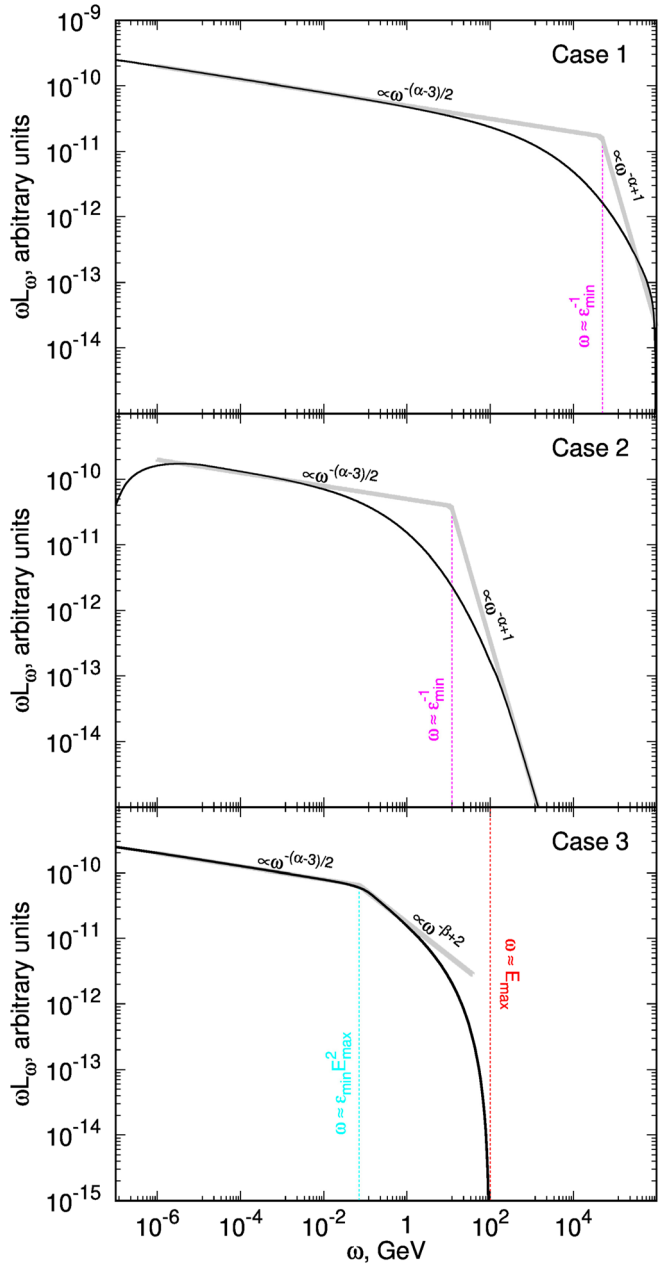


**Figure 4.** Numerical computation of IC spectrum produced on a power-law target photons with $\beta = 2.5$. Upper panel ("Case 1"): minimum and maximum energies of target photons are $\varepsilon_{\rm min} = 10^{-3}$ eV and $\varepsilon_{\rm max} = 1$ keV, respectively; the electron maximum energy was set to $E_{\rm max} = 1$ PeV. Middle panel ("Case 2"): minimum and maximum energies of target photons are $\varepsilon_{\rm min} = 10$ eV and $\varepsilon_{\rm max} = 3$ keV, respectively; the electron maximum energy was set to $E_{\rm max} = 1$ PeV. Bottom panel ("Case 3"): minimum and maximum energies of target photons are $\varepsilon_{\rm min} = 10^{-3}$ eV and $\varepsilon_{\rm max} = 1$ keV, respectively; the electron maximum energy was set to $E_{\rm max} = 100$ GeV. The electron energy distribution was assumed to be a power law with $\alpha = 3.2$ above $E_{\rm min} = 1$ MeV. The solid guide lines indicate the analytic slopes expected from Equations (45) and (35) (in the Klein–Nishina limit) and the dashed guide lines indicate the positions of spectral transformations given by Equations (45) and (49). The slope labels show the energy flux spectral indices.

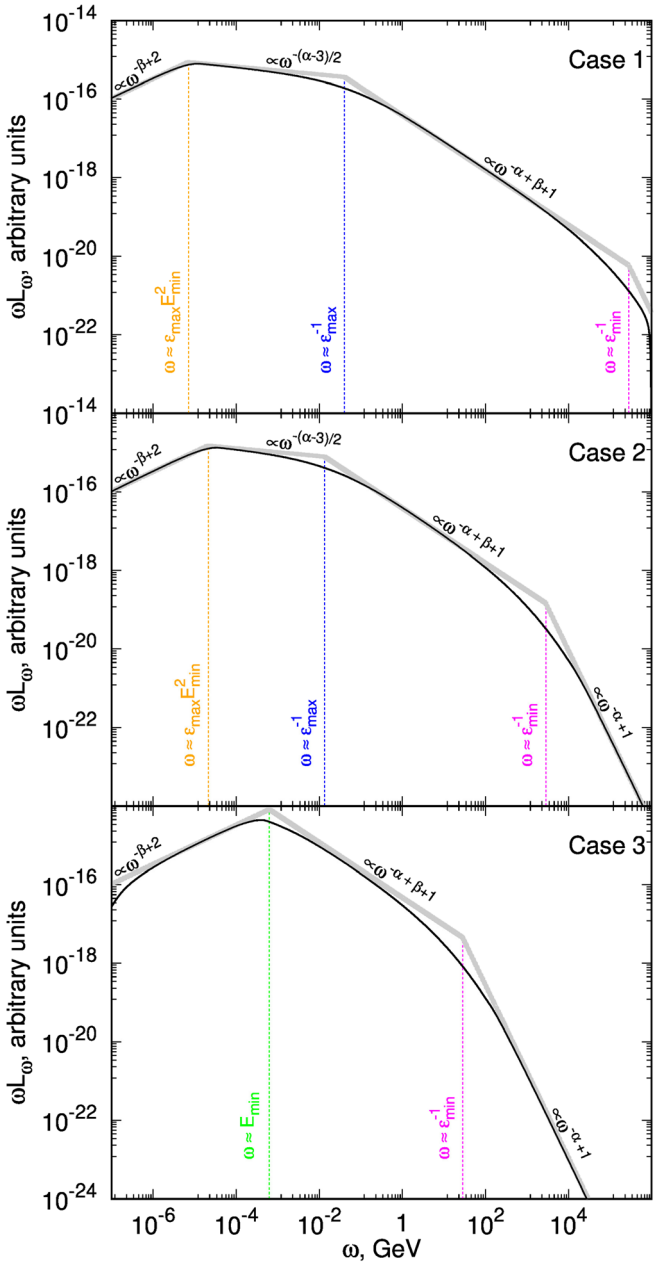


**Figure 5.** Numerical computation of IC spectrum produced on a power-law target photons with $\beta = 1.5$. Upper panel ("Case 1"): minimum and maximum energies of target photons are $\varepsilon_{\rm min} = 10^{-3}$ eV and $\varepsilon_{\rm max} = 1$ keV, respectively. Middle panel ("Case 2"): minimum and maximum energies of target photons are $\varepsilon_{\rm min} = 10^{-1}$ eV and $\varepsilon_{\rm max} = 3$ keV, respectively. Bottom panel ("Case 3"): minimum and maximum energies of target photons are $\varepsilon_{\rm min} = 10$ eV and $\varepsilon_{\rm max} = 100$ keV, respectively. The electron energy distribution was assumed to be a power law with $\alpha = 3.2$ between $E_{\rm min} = 1$ MeV and $E_{\rm max} = 1$ PeV. The solid guide lines shown are the analytic slopes expected from Equations (46) and (35) (in the Klein–Nishina limit) and dashed guide lines indicate the positions of spectral transformations given by Equations (46) and (49). The slope labels show the energy flux spectral indices.

So far, we have assumed that $\beta \neq (\alpha+1)/2$. However, this specific case deserves special mention as synchrotron emission produced by electrons having a power-law energy distribution gives rise to a power-law spectrum with photon index $(\alpha+1)/2$. In this case, all the revealed photon indexes of the IC component generated in the Thomson regime correspond to the same spectral slope, as one has

$$\frac{\alpha+1}{2} = \beta|_{\beta=(\alpha+1)/2} = \alpha + 1 - \beta|_{\beta=(\alpha+1)/2}. \qquad (50)$$

Therefore, the discussed spectral breaks vanish and the Thomson spectrum becomes a single power-law component with the standard Thomson photon index $(\alpha+1)/2$. This consideration neglects the influence of the logarithmic factors.

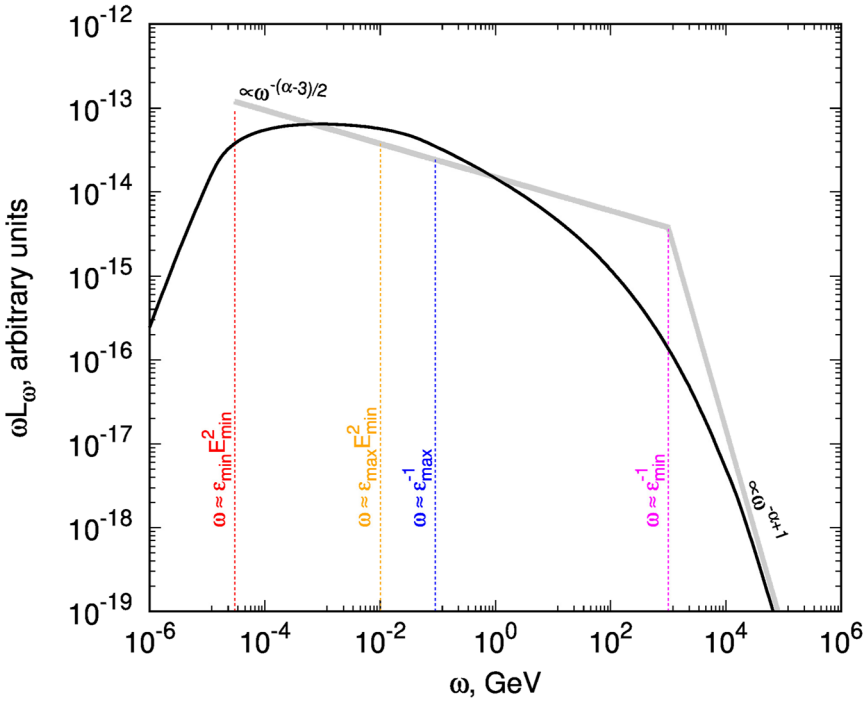


**Figure 6.** Numerical computation of IC spectrum produced on a power-law target photons with $\beta = 2.2$ between $\varepsilon_{min} = 0.1$ eV and $\varepsilon_{max} = 1$ keV. The electron energy distribution was assumed to be a power law with $\alpha = 3.4$ between $E_{min} = 100$ MeV and $E_{max} = 1$ PeV. Guide lines showing the analytic slopes expected in the Thomson and in the Klein–Nishina regimes; the positions of low- and high-energy spectral cutoffs together with "logarithmic" spectral transformations are indicate with labels. The slope labels show the energy flux spectral indices.

Accounting for these factors, one obtains

$$\dot{n}_\gamma^{\rm T} \propto \omega^{-(\alpha+1)/2} \log\left(\frac{\tilde{E}_{\rm max}}{\tilde{E}_{\rm min}}\right). \quad (51)$$

The function under the logarithm experience breaks at each of the frequencies defined by Equations (45) and (46), which causes deviations from the precise power-law dependence even if the emission is formed entirely in the Thomson regime, as shown in Figure 6.

## 4. Discussion

While the spectral properties of the IC component generated by interactions on a target that is characterized by a narrow energy distribution are well understood, such results cannot be a priori generalized to cases in which the relativistic electrons interact with a broad, i.e., a wide spread of frequencies over several orders of magnitude, distribution of photons. To reveal the "anatomy" of the IC components generated under such conditions, we have analyzed the IC scattering process on a power-law distribution of target photons analytically under the $\delta$-function approximation, verifying these findings through comparisons with the numerical integration results. We demonstrate that the generated IC component has a broken-power-law shape, where, for certain parameter combinations, we may expect up to three spectral breaks. The obtained spectral slopes depend on the power-law index of the electron distribution, $\alpha$, and on the photon index of the target photons' distribution, $\beta$. Figures 4 and 5 show that the determined analytical properties adequately reproduce the spectral properties obtained using accurate numerical calculations.

The obtained results reveal the key factors determining the spectral transitions. Under the $\delta$-function approximation, these factors are reduced to the dependence of the integration limits on the gamma-ray energy, which are summarized in Figures 2 and 3.

The analysis performed involves some simplifying assumptions. In particular, it was assumed that the target photons have a power-law distribution in the entire frequency range, between $\varepsilon_{min}$ and $\varepsilon_{max}$. At high frequencies, one often expects a relatively sharp cutoff, which can be reasonably approximated by a truncated power-law distribution. In contrast, at the lower frequency end, one often expects a presence of a cooling break, which may cause a spectral transformation.

The analysis of the influence of a cooling break (say at $E_{\rm br}$) is straightforward given that the electron distribution can be represented as

$$n_e \propto E^{-(\alpha-1)}\Theta(E - E_{\rm min})\Theta(E_{\rm br} - E) + E_{\rm br}E^{-\alpha}\Theta(E - E_{\rm br})\Theta(E_{\rm max} - E). \quad (52)$$

If one assumes that the target photons have a synchrotron origin, the photon energy distribution should also be a broken-power-law spectrum:

$$n_{\rm ph} \propto \varepsilon^{-\alpha/2}\Theta(\varepsilon - \varepsilon_{\rm min})\Theta(\varepsilon_{\rm br} - \varepsilon) + \varepsilon_{\rm br}^{1/2}\varepsilon^{-(\alpha+1)/2}\Theta(\varepsilon - \varepsilon_{\rm br})\Theta(\varepsilon_{\rm max} - \varepsilon), \quad (53)$$

where the break and cutoff positions should satisfy the following relations: $\varepsilon_{\rm min} = \varepsilon_{\rm max}\,(E_{\rm min}/E_{\rm max})^2$ and $\varepsilon_{\rm br} = \varepsilon_{\rm max}\,(E_{\rm br}/E_{\rm max})^2$.

Since Equation (38) has a linear dependence on the densities of the target photons and electrons, the resulting gamma-ray spectrum should be a linear superposition of spectra computed for each of the terms in Equations (53) and (52). The final spectrum is therefore a superposition of four components, each of which is produced by a power-law energy distribution of electrons on a power-law energy distribution of target photons,

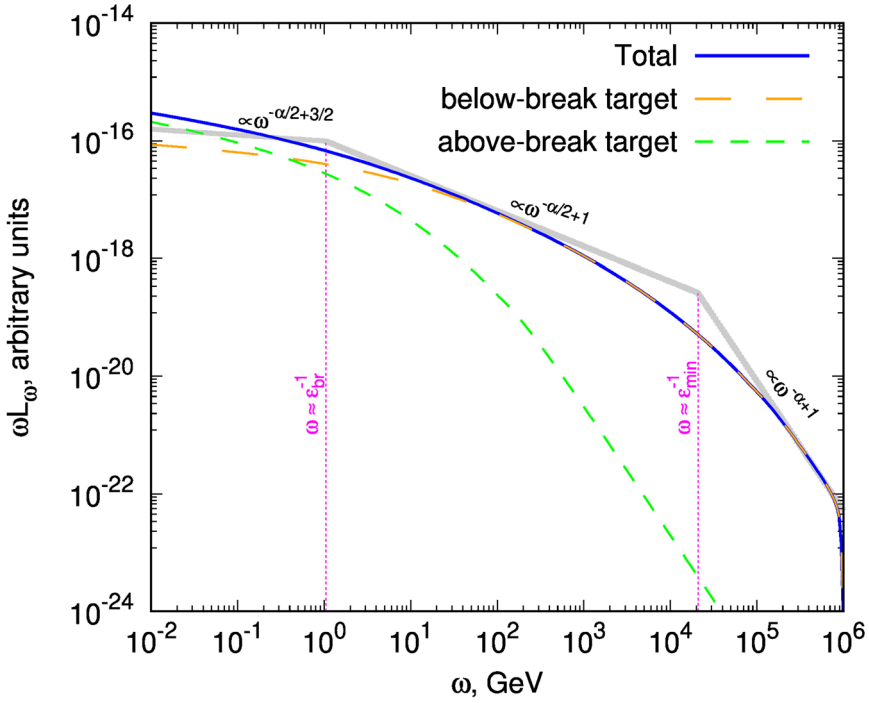


**Figure 7.** Numerical computation of IC spectrum produced on a broken-power-law target photons. The photon indexes were adopted $\beta_1 = 1.6$ and $\beta_1 = 2.1$ from $\varepsilon_{\rm min} = 10^{-2}$ eV to $\varepsilon_{\rm br} = 10$ eV and from $\varepsilon_{\rm br} = 10$ eV to $\varepsilon_{\rm max} = 1$ keV, respectively. The electron energy distribution was assumed to be a power law with $\alpha = 3.2$ between $E_{\rm min} = 1$ MeV and $E_{\rm max} = 1$ PeV. Guide lines are provided to indicate the analytic slopes expected in the high-energy part of the IC spectrum.

and thus can be obtained in the framework of the suggested approach.

Another important feature of the IC component is the transition from the Thomson to the Klein–Nishina regimes. This transformation leads to a significant spectral softening that may strongly affect the properties of the very-high-energy (VHE) emission. We have shown that if the target photon spectrum extends to sufficiently low energies, $\varepsilon_{\rm min} < m_e^2c^4/E_{\rm max}$, then the entire IC component should be dominated by photons generated in the Thomson regime; thus the Klein–Nishina effect would not cause any strong spectral softening.

To illustrate the influence of the Klein–Nishina effect, we qualitatively describe the spectral transformations expected from the above analysis for the case in which the electron distribution features a cooling break and the target photons are provided by the synchrotron mechanism. As we are focused on the high-energy part of the spectrum, we can approximate the electron distribution as a single power-law spectrum: $n_e \propto E^{-\alpha}$. As the low-energy photons define the position of the transition to the Klein–Nishina dominated spectrum, the influence of the cooling break is important for the target photons. Thus, to describe the photon distribution, we use Equation (53). When the electrons up-scatter the high-energy part of the photon target, a component with photon index $(\alpha+1)/2$ is formed (see Figure 6 for an example, but note that one should replace $\varepsilon_{\rm min}$ with $\varepsilon_{\rm br}$). This component extends to an energy $m_e^2c^4/\varepsilon_{\rm br}$, if the cooling break is formed at a sufficiently high energy, $\varepsilon_{\rm br} > m_e^2c^4/E_{\rm max}$. Above this energy, $m_e^2c^4/\varepsilon_{\rm br}$, there is a contribution from the low-energy part of the photon target, which is still upscattered in the Thomson regime. Equation (46) defines the spectral properties in this case; thus the spectrum slope is $\alpha+1-\beta=(\alpha+1)/2+1/2$ (provided that $\beta=\alpha/2$). Thus, at energy $m_e^2c^4/\varepsilon_{\rm br}$ one expects a break in the spectral index by $1/2$. At higher energies, the power-law spectrum should extend up to $m_e^2c^4/\varepsilon_{\rm min}$. Finally, if $E_{\rm max} > m_e^2c^4/\varepsilon_{\rm min}$, the IC emission should obtain the typical Klein–Nishina photon index of $\alpha+1$. This qualitative description is compared with the numerical simulations in Figure 7 from which one can see a reasonable agreement with the numerical simulations.

A broad distribution of the target photons in astrophysical sources can be formed by a superposition of blackbody components with different temperatures, e.g., from a multicolor accretion disk, or when the target photons are provided by a nonthermal radiation mechanism. Our results are applicable, with a reasonable level of accuracy, in both of these cases. However in the latter case, the target photons often offer a particularly broad power-law energy distribution over many decades in frequency. The effects discussed above therefore reveal themselves most clearly in this case. One of the most common scenarios, when a nonthermal mechanism provides target photons for IC scattering, is the so-called synchrotron self-Compton (SSC) mechanism, in which the target photons are supplied by synchrotron emission. In particular, the SSC process provides the most natural scenario for interpreting the gamma-ray emission from sources such as AGN jets (e.g., Maraschi et al. 1992) and GRBs (see Derishev & Piran 2016, and references therein). In the case of the idealized SSC scenario, that is, the electrons obey a single power-law component and exclusively up-scatter synchrotron photons, some of the revealed spectral breaks vanish and the part of the IC component formed in the Thomson regime obtains the standard slope, $(\alpha+1)/2$. There are, however, logarithmic terms that can cause a considerable deformation of this power-law behavior, as shown in Figure 6.

To make more concrete this discussion, we finish with an application of our results to a particular GRB data set. The last few years has seen exciting results in the domain of gamma-ray

astronomy, with the detection of TeV gamma-ray emission from GRB afterglows (Abdalla et al. 2019; MAGIC Collaboration et al. 2019; H.E.S.S. Collaboration et al. 2021; LHAASO Collaboration et al. 2023). For the most local of these events, GRB190829, the proximity of the GRB allowed the accurate determination of the spectral properties of the VHE emission over a broad energy range, spanning from a few hundred GeV to several TeV. The H.E.S.S. observations of GRB190829A revealed that the intrinsic[6] gamma-ray spectrum between 180 GeV and 3.3 TeV, measured approximately 5 hr after the trigger, showed no evident signs of the Klein–Nishina softening. Indeed, the spectral index of the TeV component was measured to be $\gamma_{\rm VHE} = 2.06 \pm 0.36$ (here we sum up both statistical and systematic uncertainties), which agrees well with the X-ray spectral index measured at the same epoch by the Swift X-ray telescope, $\gamma_{\rm xrt} = 2.03 \pm 0.06$ (H.E.S.S. Collaboration et al. 2021). The almost identical values for the X-ray and TeV spectral slopes suggest that the IC scattering proceeds in the Thomson regime. Even if one accounts for the uncertainties, the difference between the spectral slopes is smaller than 0.5. According to the results summarized in Section 4, the matching X-ray and VHE slopes imply that the cooling break in the synchrotron spectrum should be at sufficiently low frequencies. Since the production region moves relativistically, say with a bulk Lorentz factor $\Gamma$, the cooled synchrotron spectrum should extend below an energy of

$$\varepsilon_{\rm br} < \frac{\Gamma^2 m_e^2 c^4}{\omega_{\rm vhe}} \approx 0.1\Gamma^2 \left(\frac{\omega_{\rm vhe}}{3\ {\rm TeV}}\right)^{-1} {\rm eV}. \quad (54)$$

(Note that here the photon and gamma-ray energies are in the observer frame.)

On the other hand, the optical observation results suggest that the cooling break in the target photons appears at higher frequencies, $\varepsilon_{\rm br} > 100$ eV (Hu et al. 2021, and, e.g., Figure S5 in H.E.S.S. Collaboration et al. 2021). Thus, the minimum Lorentz factor that allows to explain simultaneously the X-ray and VHE data detected from GRB190829A is $\Gamma_{\rm min} \approx 30$. However, the self-similar solution for a relativistic blast wave (Blandford & McKee 1976) predicts for the stage of afterglow at $t \sim 5$ hr a significantly smaller bulk Lorentz factor, $\Gamma \lesssim 5$, for the conditions expected at the explosion of progenitor star of GRB190829A (e.g., H.E.S.S. Collaboration et al. 2021).

The simple analysis above allows one to reveal the limitations of one zone SSC models in explaining H.E.S.S. observations of GRB190829A. We note that a similar conclusion was obtained with Markov Chain Monte Carlo study of parameter space in the SSC scenario for this GRB (H.E.S.S. Collaboration et al. 2021).

## Acknowledgments

The authors thank the anonymous referee and V. Bosch-Ramon for useful comments and suggestions. D.K. acknowledges the support of RSF grant No. 21-12-00416. A.T. acknowledges support from DESY (Zeuthen, Germany), a member of the Helmholtz Association HGF.

## ORCID iDs

Dmitry Khangulyan https://orcid.org/0000-0002-7576-7869
Felix Aharonian https://orcid.org/0000-0003-1157-3915
Andrew M. Taylor https://orcid.org/0000-0001-9473-4758

## References

Abdalla, H., Adam, R., Aharonian, F., et al. 2019, Natur, 575, 464
Aharonian, F. A., & Atoyan, A. M. 1981, Ap&SS, 79, 321
Aharonian, F. A., Kelner, S. R., & Prosekin, A. Y. 2010, PhRvD, 82, 043002
Berestetskii, V., Lifshitz, E., & Pitaevskii, L. 1982, Quantum Electrodynamics, Vol. 4 (2nd ed.; Oxford: Butterworth-Heinemann)
Blandford, R. D., & McKee, C. F. 1976, PhFl, 19, 1130
Blumenthal, G. R., & Gould, R. J. 1970, RvMP, 42, 237
Cheng, K. S., & Zhang, J. L. 1996, ApJ, 463, 271
Crusius, A., & Schlickeiser, R. 1986, A&A, 164, L16
Derishev, E., & Aharonian, F. 2019, ApJ, 887, 181
Derishev, E. V., & Piran, T. 2016, MNRAS, 460, 2036
Felten, J. E., & Morrison, P. 1966, ApJ, 146, 686
Hu, Y. D., Castro-Tirado, A. J., Kumar, A., et al. 2021, A&A, 646, A50
H. E. S. S. Collaboration, Abdalla, H., Aharonian, F., et al. 2021, Sci, 372, 1081
Jones, F. C. 1968, PhRv, 167, 1159
Kelner, S. R., Aharonian, F. A., & Khangulyan, D. 2013, ApJ, 774, 61
Kelner, S. R., Prosekin, A. Y., & Aharonian, F. A. 2015, AJ, 149, 33
Khangulyan, D., Aharonian, F. A., & Kelner, S. R. 2014, ApJ, 783, 100
Kirk, J. G., Ball, L., & Johnston, S. 2005, ICRC (Pune), 4, 131
Longair, M. S. 2011, High Energy Astrophysics (Cambridge: Cambridge Univ. Press)
LHAASO Collaboration, Cao, Z., Aharonian, F., et al. 2023, Sci, 380, 1390
Maraschi, L., Ghisellini, G., & Celotti, A. 1992, ApJL, 397, L5
MAGIC Collaboration, Acciari, V. A., Ansoldi, S., et al. 2019, Natur, 575, 455
Schwinger, J. 1954, PNAS, 40, 132
Zabalza, V. 2015, ICRC (The Hague), 34, 922

[6] I.e., corrected for the attenuation on the extragalactic background light.